

# Pushing the Sensitivity Limits of TPS-based Continuous Deformation Monitoring of an Alpine Valley

M. Frukacz, R. Presl, A. Wieser  
Institute of Geodesy and Photogrammetry (IGP),  
ETH Zürich, Stefano-Franscini-Platz 5, 8093 Zürich, Switzerland

D. Favot, Terradata AG, Mühlestrasse 9, 8840 Einsiedeln, Switzerland

**Abstract.** Monitoring applications may require operating total stations at the limit of their sensitivity with respect to target displacements. Thorough understanding and mitigation of systematic effects is required in order to reach or push this limit.

We investigate some of these effects, in particular effects external to the total station, using data and experience gained from a continuously operating monitoring system installed at the terminus of the Great Aletsch Glacier in Switzerland. The system consists of two robotic total stations, about 60 prisms, four GNSS receivers, thermocouples, inclinometers and meteo sensors. The purpose of the monitoring is to study reversible deformations of the adjacent slopes, likely driven by snowmelt and mountain water level changes. The deformations reach the mm- to cm-level and shall be studied on time scales ranging from annual to sub-annual, and ideally even down to daily or sub-daily resolution.

Our investigation focuses on four aspects: protective housing, pillar stability, refraction, and stability of orientation, all of which were found to affect the measurements on the mm-level with lines-of-sight of up to 2 km. The results highlight signatures of apparent point displacements, and the discussion comprises approaches to bounding or mitigating these effects which may also be expected in similar monitoring situations at other locations.

**Keywords:** total station, geodetic monitoring, systematic effects, refraction, orientation

## 1 Introduction

Total stations are routinely used for geodetic monitoring if high accuracy (mm-level or better) is required, the object or area of interest can be represented by a set of marked and possibly stabilized points with line-of-sight (LoS) visibility from a sufficiently low number of specially selected instru-

ment sites. Even with potential alternatives like GNSS, laser scanners, ground-based radar or photogrammetric systems, total stations may be the best – or sometimes even the only – option in terms of sufficient sensitivity (including proper modelling and handling of uncertainties), clear interpretation of the monitoring results (in particular if the monitored points are unambiguously represented by prisms), safety, economic feasibility, and possibly further aspects. Sometimes total stations need to be operated close to or even beyond the limit of their capabilities as specified by the manufacturer in order to meet the demands of an application. An example is the monitoring system installed and gradually extended for studying short- and long-term deformations on the mm- to cm-level of the valley along the terminus of the Great Aletsch Glacier in Switzerland.<sup>1</sup>

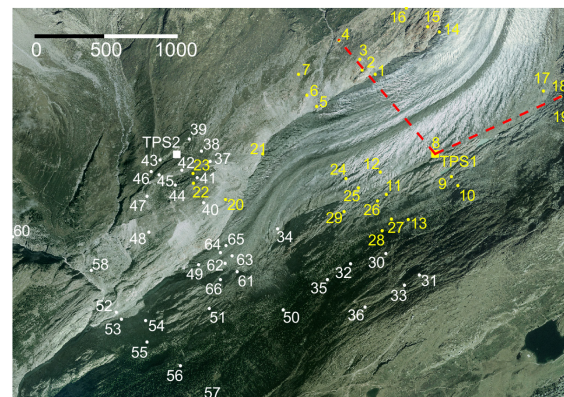


**Fig. 1** The monitoring points at the Great Aletsch Glacier and two selected profiles later used in this paper (background image © 2015 swisstopo, JD100042).

Data from two permanent GNSS stations installed in 2012 had shown annual patterns of rapid closure

<sup>1</sup> The system was installed and is operated by the Geological Institute, ETH, Engineering Geology group, with support from BSF Swissphoto and from the authors of this paper.

of the valley in spring and slow opening during autumn and winter with a peak-to-peak displacement of about 2 cm. This deformation is likely driven by snowmelt and groundwater-table changes. The geodetic monitoring system used herein was installed to further investigate the factors controlling reversible and irreversible slope displacements and deformations in the paraglacial environment of this glacier (Glueer et al., 2015).

The system now consists of two robotic total stations (TPS) each observing about 30 prisms several times per day and night, four GNSS receivers/antennas continuously collecting measurements at a 30 s data rate, meteo sensors located next to the TPS, and rock temperature sensors (see Fig. 1). One total station (TPS1) is a TCRP1201 installed in 2013 at about 1949 m a.s.l. (LoS at least 50 m above the ice, distance to prisms 42 to 1751 m, see Fig. 2), the other one (TPS2) is a TM50 installed in 2014 at about 2173 m a.s.l. (LoS at least 400 m above the ice, distance to prisms 127 to 2045 m). Both total stations were installed on pillars (see sec. 2), are remotely operated via GSM/UMTS from a server at ETH Zürich running GeoMOS, and are powered by solar panels and backup batteries. Two of the GNSS antennas are collocated with the TPS, each of them mounted concentrically (but not rotating) directly above the respective total station. The pillar and supporting rock of TPS2 have been equipped with additional sensors for the stability investigations shown in sec. 3.

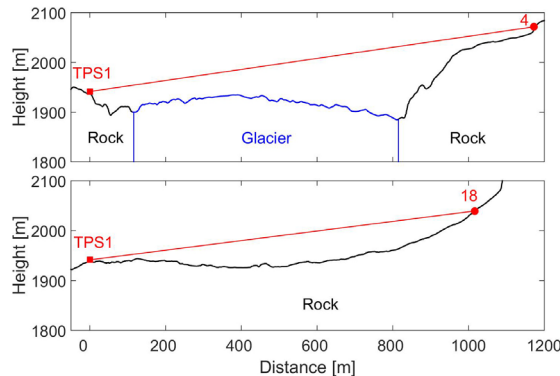


**Fig. 2** Two selected profiles along LoS from TPS1 to point 4 (across the valley) and point 18 (along the valley).

The majority of prisms are installed on profiles along the dip direction of the slopes. They are mounted directly on compact rock (gneiss and granite). The other prisms are installed in landslide areas where displacements of about 10 cm per year along

the dip direction were expected. Unfortunately, no stable areas for placing reference points were available or known beforehand. The total stations were installed in areas assumed to be stable except for the previously mentioned opening and closing of the valley.

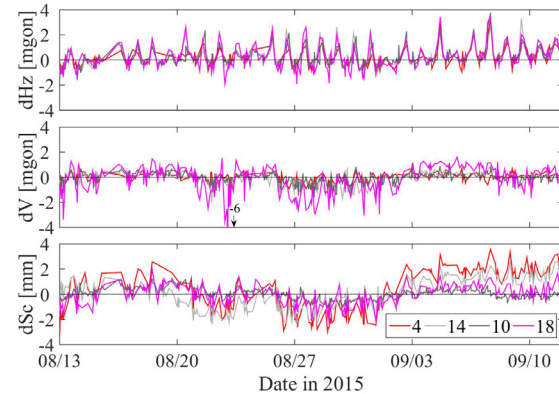


**Fig. 3** Variations of horizontal and vertical angles as well slope distances (after standard atmospheric correction) for selected points measured by TPS1 calculated with respect to the median value of the selected time period.

The measured angles and distances as retrieved from the GeoMoS database (mean of dual face measurements) vary within ranges of 4-6 mgon and 4-6 mm, respectively. Fig. 3 shows this for TPS1 and selected target points during one month in late summer 2015. We assume that most of these patterns are due to systematic deviations, not to actual displacements of the monitored points.

The angular variations reach about five to ten times the standard deviation specified by the manufacturer; the distance variations are on the level of the specified standard deviations. However, the raw observations are correlated both in space and time, as can be seen from the figure. The common daily patterns of the horizontal angles (Fig. 3, top) suggest residual orientation changes not properly accounted for during data acquisition. The largest vertical angle variations are observed for point 18 with the LoS along the valley (Fig. 2, bottom), and are likely caused by vertical refraction. The apparently systematic distance variations are likely due to residual meteorological effects (they are greatest for points at long distances measured across the valley, like 4 and 14 in Fig. 3) and possibly also to instabilities of the pillar or its support.

We will subsequently address four aspects which limit or negatively affect the accuracy of the dis-

placements extracted from the TPS measurements, namely the protective housing, pillar stability, refraction, and total station orientation.

## 2 Protective housing

The total stations were set up in remote locations, hardly accessible during the winter months, exposed to direct sunlight, harsh alpine weather conditions, potentially to animals, and easily reachable by hikers and mountaineers passing by during the summer months. So it was decided to protect the instruments in excess of their weatherproof design (IP54 and IP65, respectively) by an additional protection box consisting of plane acrylic windows and 4 posts (see Fig. 4).



**Fig. 4** TPS1 on its pillar with initial protective housing in place (picture: Geological Institute, ETH Zürich)

For a system maintenance the housing had to be removed and was then put back into place. The previous orientation and position relative to the total station were reproduced within the little slackness of the mounting screws and holes. The time series of horizontal angles of some points jumped by up to 20 mgon after this maintenance while most targets seemed not to be affected. These changes, corresponding to apparent sudden lateral displacements of some monitored points by 20 cm, were clearly non-negligible artefacts caused by the protective housing but not explainable by a tilt of the acrylic windows according to the effects of a plane parallel plate.

An exact replica of the housing and a suitable experimental setup in the geodetic metrology laboratory of IGP (Fig. 5) were used to investigate the effect of the housing on the total station measurements. In particular measurements to a fixed prism about 50 m from the total station were made and recorded while the protective housing was rotated stepwise about its vertical axis, collinear with the

total station's vertical axis. For comparison the process was repeated with the acrylic panes removed from the housing, and subsequently also with different total stations.

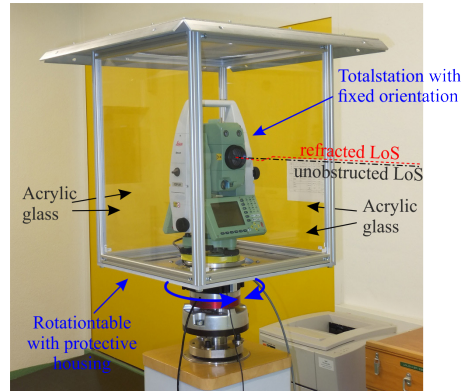


**Fig. 5** An experimental setup to investigate the impact of protective housing on the TPS measurements.

Fig. 6 shows the variations of the measurements obtained during one such experiment. The blue lines correspond to the TCRP1201 measurements without acrylic windows (but with the frame and posts of the protective box still in place). The measurements are mostly constant apart from random noise well within the specification of the instrument. However, the horizontal angles are heavily and systematically affected when the box is rotated by about 45 gon either way from the LoS to the prism. The reason is obstruction of the prism (target) by the posts. The automatic target recognition algorithm does not detect (and flag) the problem until the obstruction exceeds a certain limit. In this test, the corresponding error, not detectable from the total station output alone, reaches about 6 mgon. The distance and vertical angle measurements are not affected by the partial obstruction, as may be expected since the posts are vertical.

With the acrylic windows inserted the measurements are systematically affected, in particular the distances and horizontal angles. All three instruments (TCRP1201, MS50, S8) show a very similar behaviour except for certain effects close to the region where the LoS is approximately perpendicular to the window surface. There, the S8 does not output measurements within a cone of about  $\pm 3$  gon, while the target recognition of the MS50 is still active but produces outliers of horizontal and vertical angles within a region of about  $\pm 0.5$  gon. The measurements of the TCRP1201 mainly exhibit

higher noise in the immediate vicinity of the window's surface normal.<sup>2</sup> The offset and non-linearity of the distance variations (Fig. 6, bottom) is fully explained by the thickness, refractive index and varying rotation angle of the window. The asymmetry and non-linearity of the horizontal angle variations and the fact that they are nowhere 0 indicates that the acrylic window is not plane parallel. We could reproduce the error pattern numerically by assuming that the window is slightly wedge-shaped. Non-parallelism of only a few hundredth of a mm was enough to explain the effect that we had found.

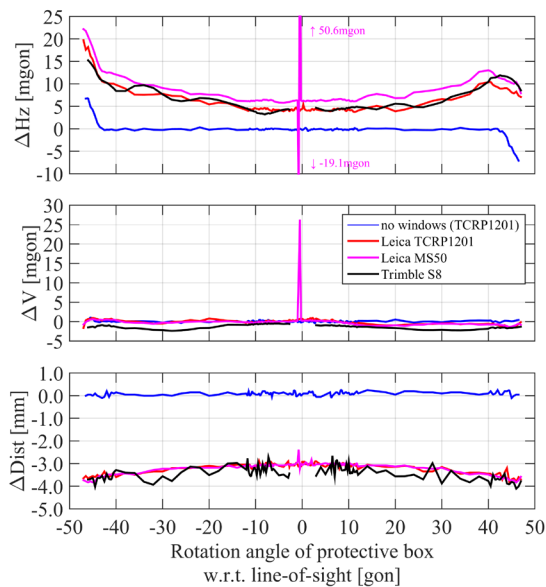


**Fig. 6** Variation of total station measurements as a function of angle between LoS and housing (surface normal of acrylic window); denser sampling for almost perpendicular line-of-sight (0 rotation angle) and for angles beyond 40 gon.

The increased deviations towards both ends of the curve are caused again by the posts. The smaller scale variations differing between the instruments persisted with independent repetition of the experiment and are most likely due to local inhomogeneities of the windows both in terms of geometry and refractive index which affect the instruments differently because of the different target recognition technology (including effective spatial low-pass filtering by the finite diameters of the optical beams).

<sup>2</sup> These situations can of course be avoided in a real-world monitoring application by tilting the respective window sufficiently w.r.t. LoS, and in fact practitioners have known this for a long time.

The reason for the jump of the measurements of TPS1 after the maintenance was thus due to partial obstruction of LoS by the posts. However, the lab investigation showed that an additional housing may critically impair the monitoring system even if such obstructions are avoided. The horizontal angle errors change with changing angle between LoS and window surface by up to  $0.4 \cdot 10^{-3}$  mgon/mgon (except in the immediate vicinity of the posts, where they are higher). While this may be uncritical for many monitoring applications, it may result in significant errors of the estimated displacements if the window is replaced, if its orientation changes because of external influences or work, or if a target point moves by more than about 0.5 gon (0.8 m at a distance of 100 m).

We found qualitatively similar results with high quality glass instead of acrylic, and significantly worse results with an acrylic cylinder instead of the planar windows. Ideally, if an additional protection is required at all, the measurements should be made through sufficiently big holes in the housing rather than through any kind of transparent material. We have also investigated this using an experimental setup like before, and found that the diameter of the holes should be larger than the aperture of the telescope to avoid systematic errors on the level of mgon to tens of mgon caused by partial obstruction or distortion of the measurement beams when they touch or overlap the border of the holes. For the total stations mentioned above we found that holes of at least 50 mm diameter should be drilled at the required locations to account for instrument beam width, potential target point displacements, and for limited precision of the hole's location w.r.t. the total station once the entire system is mounted. The housing within the above monitoring system was replaced by opaque cylinders with such holes.

### 3 Pillar stability

Both total stations are mounted on 1.5 m high aluminum pillars consisting of two concentric pipes with no mechanical connection between the outer and inner one. They are screwed down independently on bedrock with bolts glued into the rock. The outer pillar serves for radiation and weather protection and has vents for air circulation. The inner one has a diameter of 0.21 m and carries both the total station and the GNSS antenna.

To investigate potential pillar instabilities or deformations and their impact on the total station measurements TPS2 was equipped with additional sensors. Calibrated thermocouples were equally distributed around the circumference of the inner pipe at 3 different heights and within vertical profiles. A biaxial geotechnical inclination sensor (Jewell D711-2B,  $\pm 5^\circ$  range, temperature calibrated by the manufacturer) was mounted directly on the rock supporting the pillar. Two single axis inclination sensors (Wyler Zerotron Type-3,  $\pm 10^\circ$  range) were connected to the top of the inner pillar in an orthogonal configuration. Additionally, a meteorological sensor measuring a variety of parameters was temporarily installed at this site.

The measurements of the Jewell sensor show that the solid rock supporting the pillar is not perfectly stable but tilts in correlation with solar radiation and air temperature. Fig. 7 shows a time series of inclination measurements, air temperature and solar radiation during one week in Oct/Nov 2015. The tilt increases towards North by up to  $20''$  with a clear diurnal pattern closely resembling the variations of air temperature and solar radiation. There is a smaller inclination towards West in the morning and towards East in the evening. The inclination recorded by the inclination sensor of the total station agrees well with the rock inclinations in terms of signature and sign, but it is larger by up to  $10''$ .

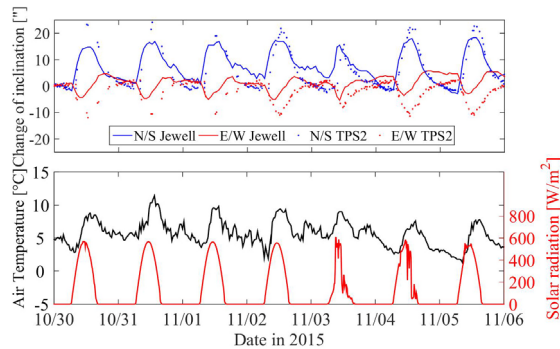


**Fig. 7** Variation of rock inclination (Jewell) and total station tilt (TPS2) North/South and East/West directions at site TPS2 (top), and air temperature and solar radiation (bottom).

We expected that this might be due to pillar bending. However, a calculation of the pillar deformation using a finite element model (FEM) and the actually measured temperature differences within the pillar did not fully explain the difference. The temperature differences within horizontal sections of the pillar (i.e. along the circumference) were typ-

ically well below  $1^\circ\text{C}$  (they were up to about  $3^\circ$  within the vertical profiles, which is not relevant for pillar bending). The deformations predicted by the FEM software corresponded to inclination changes of  $3\text{--}5''$  or less between the bottom and the top of the pillar.

The residual difference between the sensed inclinations can be due to pillar tilt (at its base), uncompensated temperature effects of the sensors involved, or unbalanced thermal expansion effects of the tribrach or total station. Unfortunately, data from the inclination sensors (Wyler) on the top of the pillar, from those in the rock and from the thermocouples could not be collected at the same time, and additionally the sensors on the top of the pillar and their consoles were exposed to direct sunlight, which increased the noise level significantly and possibly also biased their measurements. So a direct comparison and clarification of the reason for the apparent additional inclination of the total station was not yet possible. However, the available data from the Wyler sensors suggest that there may actually be a discrepancy of a few arcseconds between the top of the pillar and the total station.

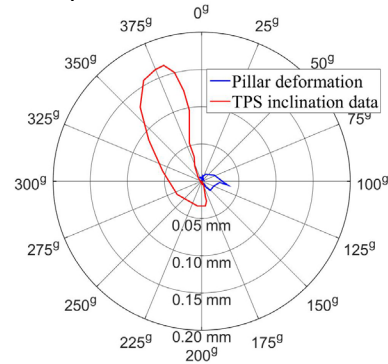


**Fig. 8** Displacement of TPS2 corresponding to the total station tilt measurements of 08/30/2015 assuming a rigid pillar and tribrach (red), and contribution by pillar bending as estimated from FEM and thermocouple measurements (blue).

The total station's measurements are not directly affected by the small tilts discussed so far because of the internal inclination corrections. However, tilt of rock, pillar, and instrument, and bending of the pillar also cause a displacement of the total station's reference point. A numerical analysis assuming that the pillar, tribrach and total station are perfectly rigid and the tilt variation indicated by the total station thus represents the tilt variation of all 3 elements, yields horizontal displacements of the total station of less than 0.2 mm, predominantly towards

North-North-West (see Fig. 8), which is also the direction of the steepest uphill slope. The pillar bending as resulting from the FEM analysis is even less. So these effects will very likely be buried within noise and other systematic deviations of the total station measurements.

However, so far it is not known how the rock deforms in response to temperature and radiation changes, and thus the rock tilt changes mentioned above cannot be transformed into equivalent displacements of the total stations. We must expect that the diurnal patterns due to this effect are of the same order of magnitude as the 0.2 mm estimated above, or even larger. Fig. 7 shows that the rock tilts are relatively constant during and between the nights. This is one motivation to use primarily measurements obtained during the night for highly sensitive deformation and displacement analysis.

Using the FEM and the available temperature measurements of the pillar, diurnal height changes of the pillar of typically around 0.5 mm but up to 1 mm (with 30 K temperature differences between day and night) were predicted. For nearby target points (distance of a few 100 m) this may noticeably affect the vertical angle measurements (on the level of a few 0.1 mgon) and may warrant correction of the measurements for this time-varying vertical eccentricity. An additional eccentricity of at least the same order of magnitude may be caused also by thermal expansion of the supporting rock, and further investigations would be required to clarify its impact. However, refraction will mask all these effects for larger distances.

#### 4 Atmospheric refraction

The effects discussed in sec. 2 and 3 do not explain the systematic variations of the zenith angles and distances visible e.g. in Fig. 3. Most likely they are caused by residual atmospheric refraction. However, mitigating these refraction effects using numerical models is not possible because the atmospheric parameters are not known or observable with sufficient spatial and temporal resolution. In this section we will instead roughly estimate the magnitude and variability of the expected refraction effects using approximations, assumptions and available meteo data and thus assess whether the unexplained variations of the actual measurements can plausibly be attributed to refraction.

Meteorological data relevant for this study are available from: (1) two STS meteo-sensors (air temperature and barometric pressure) located next to the TPS and used to record measurements every 30 minutes for correction of the raw TPS measurements within the GeoMoS software; (2) MeteoSwiss stations Bruchji (2300 m a.s.l.; air temperature and precipitation) and Eggishorn (2893 m a.s.l.; temperature, pressure, humidity, solar radiation) with 10 minutes time resolution, see Fig. 9; (3) sensors for rock-temperature and air-temperature 0.15 m above-rock, installed on selected locations at the South and North slope of the valley and recording measurements with 30 minutes time resolution.

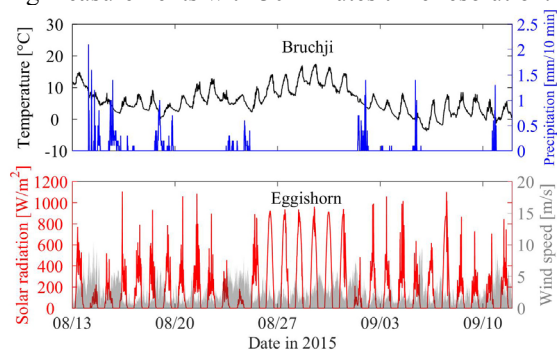


**Fig. 9** Air temperature (black), precipitation (blue), solar radiation (red) and wind speed (grey) at two nearby MeteoSwiss stations (Source: MeteoSwiss).

From these data vertical temperature gradients  $\tau$  (lapse rates, in K/m) were roughly estimated as a function of time  $t$  and height  $h$  above ground assuming that the exponential relation (Brooks, 1948):

$$\tau(h, t) = a(t) \cdot h^{b(t)} \quad (1)$$

holds within the entire monitoring area. The time series of  $a$  and  $b$  were calculated for epochs 30 minutes apart using the temperature measurements within the rock and 15 cm above the rock (assumed to represent the lapse rate at 7.5 cm above ground) at a location close to prism 17, and the temperature measurements at the two MeteoSwiss stations (assumed to represent the lapse rate at 300 m above ground).

The result is shown in Figs. 10 and 11 for the vicinity of TPS1 and one month in summer 2015. Just above the ground the estimated lapse rate has a very high magnitude (exceeding -50 K/m, Fig. 10) and significant diurnal variations (up to 10 K/m, Fig. 11). The daily variations and the magnitude of the lapse rate decrease with increasing distance from the ground. Even though the above assumptions can

only be very rough approximations to the real temperature gradients, this pattern is realistic and the typical lapse rate of a glaciated alpine valley ( $-0.005$  K/m, see Rolland, 2003) is reached at about 300 m above the ground. It is worth mentioning that the expected temperature inversion during the nights was not observed except during one single night (08/24-25) after a cloudy day with wind and rain.

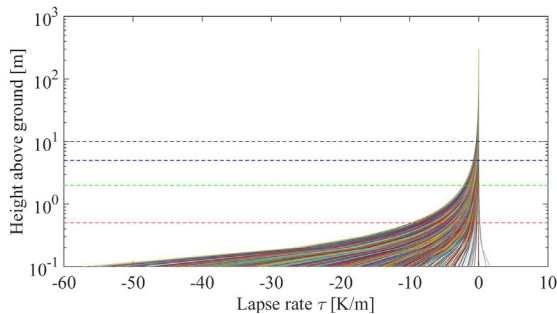


**Fig. 10** Estimated temperature gradient as a function of height above ground in the vicinity of TPS1 for the time covered by Fig. 9; each line corresponds to an epoch with 30 min time resolution.

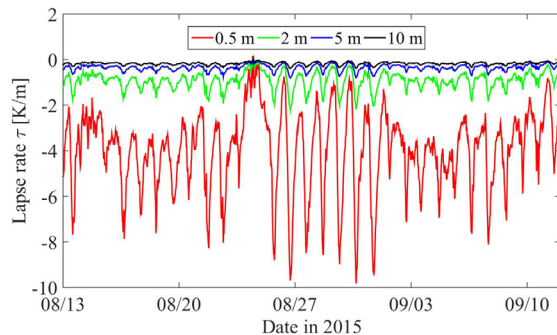


**Fig. 11** Time series of estimated temperature gradients at the vicinity of TPS1 and 4 selected heights above ground.

When adapting these models, we do not take into account the cooling effect of the melting as mentioned in Van den Broeke (1996). This effect extends to a height of about 100 m above the glacier with the most pronounced effects within the first 20 m where it causes an inverted lapse rate of about  $0.7$  K/m during sunny summer days. We ignore this effect because the LoS in our case are high above the glacier.

Using the above meteo data and temperature gradient model, pressure gradients calculated from the meteo data, a refractive index model (Ciddor, 1996; Ciddor and Hill, 1999) taking into account the respective wavelengths, and using a digital terrain

model of the monitoring area (Swisstopo model with  $2 \times 2$  m<sup>2</sup> grid size, densification with own laser scanning measurements in the vicinity of the total stations) we estimated the refraction effect on the zenith angles and distances by ray-tracing. The software was written in Matlab. For each target and epoch meteo-parameters and gradients were calculated for points equally spaced along the chord using the above models. Taking into account the DTM resolution, the limited accuracy of the modeled meteorological parameters, the computational effort and the purpose of the calculations (order of magnitude), we chose a step size of 1 m for the numeric integration along the chord. In Figs. 12 and 13 we show the resulting zenith angle and distance variations for one month in summer 2015 and for two representative LoS, as previously shown in Fig. 2: one across and one along the valley. For comparison we also plotted the variation of the real total station measurements.

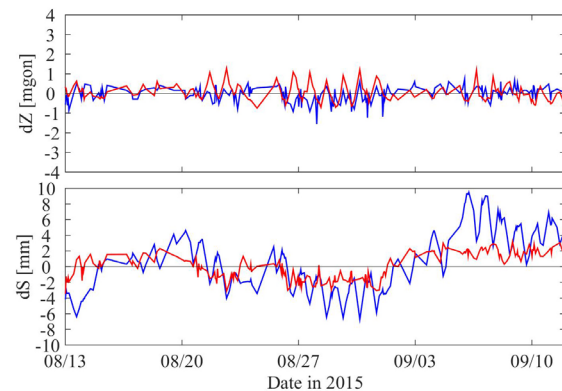


**Fig. 12** Refraction effect (red) predicted for zenith angle (top) and residual refraction effect of distance after ray-tracing (bottom) of point 4 observed from TPS1 at approx. 1200 m across the valley; variation of actual TPS measurements (blue) w.r.t. long term median shown for comparison.

As can be seen the variations of the predicted zenith angles have a magnitude of about 1 mgon for the sighting across and 3 mgon for the sighting along the valley. They are in good agreement with the magnitude of the actually observed vertical angle variations which suggests that these indeed are due to vertical refraction. It is plausible that the effect is much smaller for the sighting across the valley (Fig. 12) than along (Fig. 13), because the LoS stays close to the ground and thus within an area of strong vertical temperature gradient in the latter case, while it is mostly far from the ground

and thus within an area where the vertical refraction is dominated by the (much less variable) pressure gradient in the former one.<sup>3</sup>

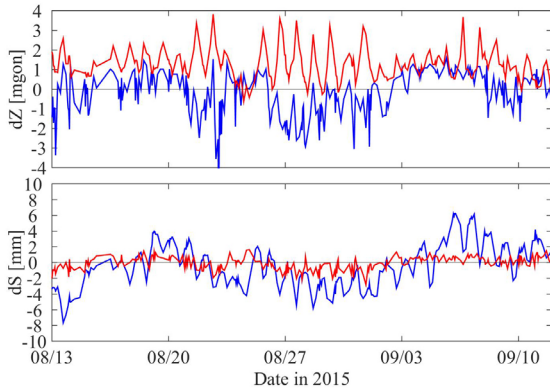


**Fig. 13** Refraction effect (red) predicted for zenith angle (top) and residual refraction effect of distance after ray-tracing (bottom) of point 18 observed from TPS1 at approx. 1000 m along the slope of the valley; variation of actual TPS measurements (blue) w.r.t. long term median shown for comparison.

The long-term variations of the distance measurements are well represented by the ray-tracing results. However, standard meteo correction based on temperature and pressure close to the instrument would yield almost identical results since the simplified meteo model underlying the ray-tracing does not reflect the actual temperature distribution along the LoS. The major variations of the actually observed distances (Figs. 12 and 13 bottom, blue) are short term, in particular with diurnal patterns, and much larger than the variations explained by the ray-tracing. With distances of about 1 to 1.2 km the deviations between ray-tracing results and actual variation are up to about 4 mm. This indicates that the actual average temperature along the LoS differs by up to about 4 K from the modeled one (and from the temperature measurements at the TPS site). This may be due to different exposure to sunlight, to the cooling effect of the glacier mentioned previously, and perhaps also to non-optimum location of the meteo-sensors near the total stations. Taking into account the striking similarity of the variations of the measured distances across and along the valley, it seems possible to mitigate these variations either

<sup>3</sup> As stated above it is not possible to calculate sufficiently accurate refraction corrections because the meteo data (including gradients) are not available along the LoS and for the exact time of the measurement.

by estimation of a time-varying local scale factor or by improved meteo corrections based on additional meteo measurements near some of the prisms.

## 5 Orientation

For data collection a nearby prism (i.e. one with high probability of being actually found and measured) was selected in GeoMoS as orientation target. However, the horizontal angles of each individual target point obtained with this approximate orientation vary within a range of 1-2 mgon during the nights, and by up to 4 mgon during the days, for some points even more. Clearly, a better orientation solution is required avoiding extrapolation, providing redundancy, and assuring long-term stability of the orientation. As mentioned previously, this is not straightforward in this monitoring system because no stable points were known beforehand. GNSS data are available at the TPS sites but there are not yet any prisms collocated with GNSS antennas. So, the reference points defining the total station's orientation have to be determined using the TPS alone data.

Although there is no geometric redundancy and the expected accuracies of the points are very inhomogeneous being a linear function of the distance, data of TPS1 were processed according to a strict deformation analysis based on the Hannover method (Niemeier, 1985) using the Panda software.<sup>4</sup> Data from selected nights 10 days to 3.5 months apart were chosen for pairwise analysis. The results of one such pair, shown in Fig. 14 are representative: all points on the north-west slope were classified as reference points, i.e., as stable, while all points on the same side of the valley as the TPS were classified as object points, i.e. as not stable. The indicated displacement of the TPS station corresponds approximately to its displacement as resulting from the independent GNSS data analysis (about 15 mm in a direction of about 293°), and the bigger displacement of points 24-29 in the direction of the down-hill dip is plausible since these points are located on an active landslide. The common displacement of the southern points in Fig. 14 would be explainable by the closing of the valley mentioned in the introduction. GNSS data of TPS2 were not yet available for that period of time. However, data from the following year suggest that indeed there may be no or significantly less corre-

<sup>4</sup> <http://www.geotec-gmbh.de/en/panda/>

sponding displacement of the north side of the valley, such that the classification of all those points as stable may be correct.

However, a detailed comparison of these results with the GNSS time series shows that only the North component (of about 12 mm) is almost identical while the East component differs by more than 5 mm and the TPS results of all epochs analyzed indicate significantly more westward displacements of than shown by the GNSS results. The lack of actually stable reference points and the inhomogeneous accuracy within the observed point field (with larger error ellipses and thus decreased sensitivity for the points across the valley) mean that the Hannover method using only the TPS measurements is not sufficient.

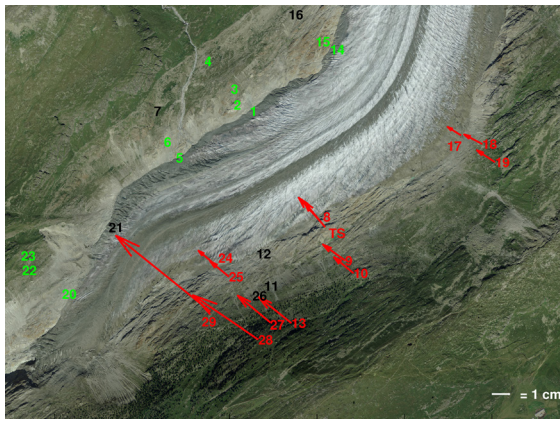


**Fig. 14** Displacements obtained using Hannover method between two selected epochs (04/13/2014 and 07/31/2014). The red arrows identify the displacements of the object points of TPS1, identified as instable with 95% probability using the Hannover method. Object points are labeled in red, reference points in green; black points do not have enough observations for a comparison (background image © 2015 swisstopo, JD100042).

Based on the available data it seems more reasonable to use a low-pass filtered time series of GNSS coordinates to express the TPS coordinates in a stable reference frame, and to calculate the orientation from the network.<sup>5</sup> Assuming that the points within the profiles are displaced only by the closing and opening of the valley and thus within the profile, it seems straightforward to define the orientation by the average direction of the prisms in the same pro-

<sup>5</sup> Ideally some prisms should be collocated with GNSS antennas to derive the orientation within the same stable reference frame. This is an envisaged future extension of the network.

file as the TPS. However, we have chosen to find a suitable set of prisms by analyzing the real measurements (processing only data obtained during the nights because of less variability).

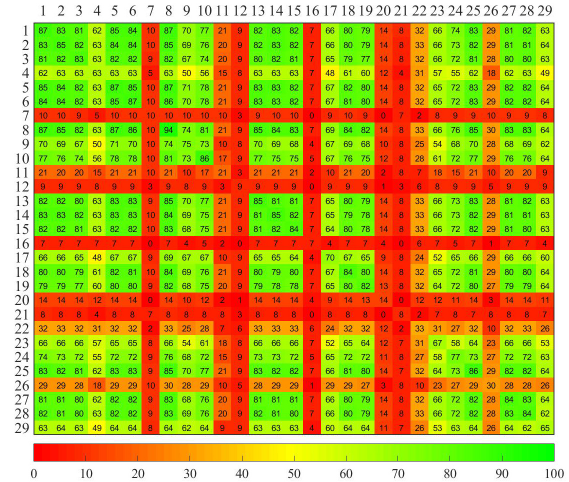


**Fig. 15** Angle availability (%) for period 03/15-08/03.2014.

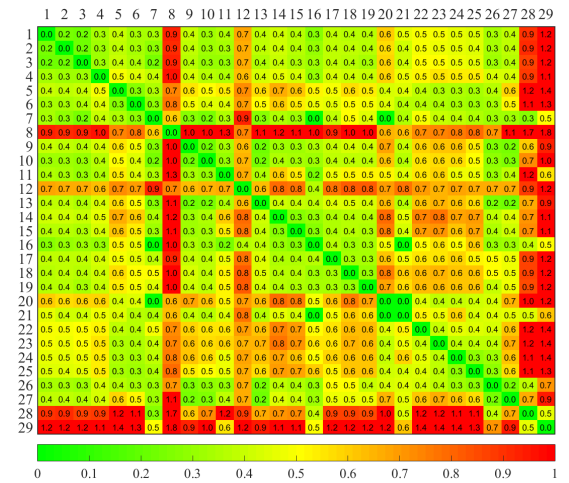


**Fig. 16** Empirical standard deviations (mgon) of horizontal angles for period 03/15-08/03.2014.

The approach was based on an analysis of the availability and empirical standard deviation of the orientation as resulting from a chosen subset of points. For preselection of points, the time series of horizontal angles  $\alpha_{i,j}$  were calculated for all pairs of points  $i$  and  $j$  and for the period March to August 2014. Using the median and the median absolute deviation (MAD), outliers were identified and removed from the time series. Then the availability (percentage of epochs at which the angle is available) and the empirical standard deviation of the an-

gle were calculated. These results were visualized for all pairs of points (see Figs. 15 and 16). Points associated with high availability and low standard deviation of angles were chosen as candidates for the orientation calculation.<sup>6</sup>

Then an exhaustive search over all possible combinations of at least 5 out of the 18 points remaining after the above preselection was carried out analyzing the availability and precision of the orientation when calculated from the respective subset of points. For each epoch the orientation was considered available if it could be computed from at least 5 target points (outliers again removed using median and MAD, but only within the respective epoch). The precision was measured by calculating the empirical standard deviation and that of the estimated (mean) orientation within each epoch, and finally selecting the 95<sup>th</sup> percentile of the standard deviations of the estimated orientations.

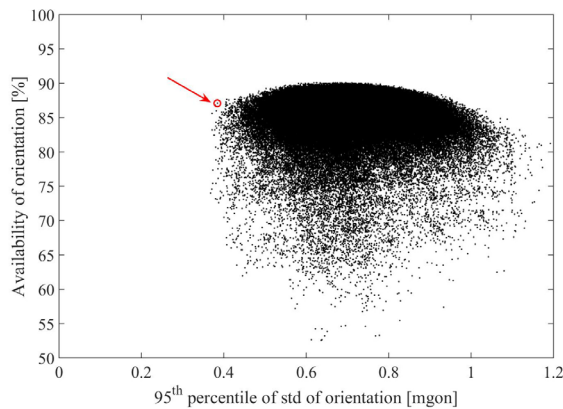


**Fig. 17** Availability and 95<sup>th</sup> percentile of standard deviation of orientation for all candidate sets of orientation points based on data from 03/15-08/03/2014; selected optimum candidate indicated by arrow.

The result is displayed in Fig. 17. Obviously there is a trade-off between high availability and low standard deviation, and a further criterion is needed to retrieve an optimum set of points based on this multi-objective optimization. We selected the set whose quality is indicated by the arrow in Fig. 17: it corresponds to points {1, 2, 3, 4, 9, 10, 13, 17, 27} with an orientation availability of 87% and standard deviation of the orientation better than 0.38 mgon in 95% of the cases. As the figure shows, (slightly) higher availability is only achievable at the cost of (much) higher standard deviation while (slightly)

<sup>6</sup> Arbitrarily, a 50% availability threshold and an 0.6 mgon standard deviation threshold were used for this selection.

lower standard deviation is only achievable at the cost of (much) lower availability; the chosen solution is an inflection point on the Pareto front and therefore optimum (see e.g., Domingo-Perez et al., 2016).<sup>7</sup>

Using Fig. 14 we see that the set of orientation points identified using the above algorithm comprises mostly the points located within the same profile as TPS1, and two more points located on the same side of the valley as TPS1 and thus subject to almost the same displacements as far as closing and opening of the valley is concerned. So it is plausible that this choice is useful to establish a stable orientation reference, furthermore – based on the above analysis – it is also clear that it does so with high availability. Fig. 18 shows the horizontal angles of a point (10) after application of the orientation calculated from the above subset of points. The result is representative for all points. It shows that short and long-term variations of the horizontal angle are successfully mitigated. The remaining noise is fully explained by the standard deviation of the angle measurements. A corresponding study for TPS2 is yet to be carried out.

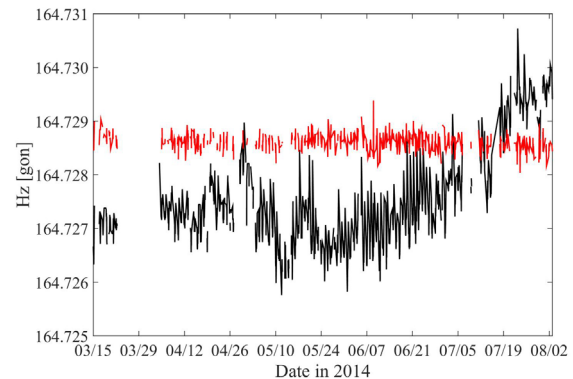


**Fig. 18** Time series of horizontal angles of point 10 before (black) and after (red) application of the orientation calculated from the above orientation points.

## 6 Conclusion

We have analyzed various systematic effects deteriorating estimated displacements calculated from total station (TPS) measurements in an alpine environment.

<sup>7</sup> The same optimum solution has also been found with much less computational effort by starting from the subset of 18 candidate points, iteratively removing the one contributing most to the empirical standard deviation of the orientations, and stopping once there were only 9 points left.

We showed why an additional housing of a TPS with windows should be avoided if possible; partial obstruction of the field-of-view and reflections from the windows may go unnoticed by the instrument and may cause deviations exceeding the instrument specifications by 1-2 orders of magnitude. If housing is necessary, holes larger than the aperture of the telescope should be drilled and the measurements should be taken through these holes.

The solid rock supporting the pillar of one of the TPS was found to have diurnal tilt variations on the level of 10'' which might cause significant total station displacement. Further displacements due to potential bending of the pillar (horizontal temperature gradients up to 1 K were found within the double layer pillar) or tilting of the pillar and instrument were found to be on the level of 0.2 mm or less and thus usually negligible. For nearby targets the temperature induced pillar height variations of up to about 1 mm might have to be taken into account using numeric eccentricity corrections.

Vertical angle variations up to about 1 mgon for lines-of-sight (LoS) of about 1 km were predicted due to vertical refraction across the valley, and up to about 3 mgon for LoS along the valley using a simplified model based on actual meteorological observations. It corresponded well to the actual variations of the measurements in terms of order of magnitude and temporal variability. Correlated short-term distance variations of 2-4 ppm were found for all LoS across and along the valley suggesting that it may be possible to reduce them using a time-dependent scaling factor.

Using a multi-objective optimization approach, a set of points was identified for determination of the total station orientation. The horizontal angles measured to these points are mostly unaffected by annual opening and closing of the valley, such that this orientation may be combined with GNSS-derived position updates of the TPS sites in order to establish a suitable geodetic datum for deformation analysis.

Future extensions of the network should include prisms collocated with GNSS antennas in order to (i) support datum definition, and (ii) possibly provide reference distances for local scale factor estimation despite the annual deformation signals.

## Acknowledgement

The authors thank Simon Löw, Franziska Glüer, Reto Seifert and Lorenz Grämiger from the Engineering Geology Group, ETH Zürich for granting access to data from various sensors installed and operated by them, and for the cooperation during field trips.

## References

- Brocks K. (1948). Über den täglichen und jährlichen Gang der Höhenabhängigkeit der Temperatur in den unteren 300 Metern der Atmosphäre und ihren Zusammenhang mit der Konvektion. *Berichte des Deutschen Wetterdienstes in der US-Zone*, Nr. 5 (in German).
- Ciddor P.E. (1996). Refractive index of air: new equations for the visible and near infrared. *Appl Optics* 35: 1566-1573.
- Ciddor, P.E. & Hill, R.J. (1999). Refractive index of air, *Applied Optics* 38: 1663-1667.
- Domingo-Perez, F., Lazaro-Galilea, J.L., Wieser, A., Martin-Gorostiza, E., Salido-Monzu, D., de la Llana, A. (2016). Sensor placement determination for range-difference positioning using evolutionary multi-objective optimization. *Expert Systems With Applications*, 47, 95-105.
- Glueer, F., Loew, S., Seifert, R., Frukacz, M., Wieser, A. (2015). Design and operation of a comprehensive and permanent rock slope deformation monitoring system at the Great Aletsch Glacier (Switzerland). *Geophysical Research Abstracts*, Vol. 17, EGU General Assembly 2015.
- Niemeier, W. (1985). Deformationsanalyse. In: Pelzer H (ed) *Geodätische Netze in Landes- und Ingenieurvermessung II*. Konrad Wittwer, Stuttgart, 559-623.
- Rolland, Ch. (2003). Spatial and Seasonal Variations of Air Temperature Lapse Rates in Alpine Regions. *Journal of Climate*, 16, 1032-1046.
- Van der Broeke, M.R. (1997). Structure and diurnal variation of the atmospheric boundary layer over a mid-latitude glacier in summer. *Boundary-Layer Meteorology*, 83, 183-205.